INFLUENCE OF Sn ON THE MICROSTRUCTURE AND MECHANICAL PROPERTIES OF Ti-Mo-Nb ALLOYS FOR ORTHOPAEDIC APPLICATIONS

N. Muchavi[1,2,*], L. Raganya[1], R. Machaka[3], G. Motsi[1,4] & E. Makhatha[2]

ARTICLE INFO

Contact details
∗   Corresponding author
    emakhatha@uj.ac.za

Author affiliations
1   Advanced Materials and Engineering, Manufacturing Cluster, Council for Scientific and Industrial Research, Pretoria, South Africa

2   Department of Metallurgy, School of Mining, Metallurgy and Chemical Engineering, University of Johannesburg, Johannesburg, South Africa

3   IdyaFactory Co., New South Wales, Australia

4   Department of Materials Science and Metallurgical Engineering, University of Pretoria, Pretoria, South Africa

ORCID® identifiers
N. Muchavi
0000-0001-9951-2054

L. Raganya
0000-0002-3259-8647

R. Machaka
0000-0002-3174-8703

G. Motsi
0000-0003-0094-5998

E. Makhatha
0000-0003-2157-9712

ABSTRACT

Metastable ß-Ti alloys intended for orthopaedic implants typically possess undesirable a', a'', ω precipitates, which increase the elastic modulus. Non-toxic Sn was reported as an effective suppressor of a', a'' and ω precipitates. Furthermore, increasing Sn content was reported to decrease the elastic modulus. In this study, the cluster plus glue atom (CPGA) model was used to develop structurally stable β-Ti alloys through the addition of Sn. Arc melting was conducted to fabricate the alloys. The effect of substituting Mo atoms with 0.4 and 0.5 Sn atoms on the microstructure and mechanical properties of $[(Mo,Sn)(Ti)_{14}](Nb)_1$ alloys was investigated. The microstructure of the alloys exhibited large equiaxed beta grains with the $[(Mo_{0.6}Sn_{0.4})(Ti)_{14}](Nb)_1$ and $[(Mo_{0.5}Sn_{0.5})(Ti)_{14}](Nb)_1$ alloys showing substructures. The XRD results showed that the alloys consisted of the β phase; however, the presence of a'' was observed in the $[(Mo_{0.6}Sn_{0.4})(Ti)_{14}](Nb)_1$ alloy. The study showed that substitution of 0.5 Mo atoms with 0.5 atoms of Sn to form the $[(Mo_{0.5}Sn_{0.5})(Ti)_{14}](Nb)_1$ cluster resulted in an elastic modulus of 49 GPa.

OPSOMMING

Metastabiele β-Ti-legerings bedoel vir ortopediese inplantings besit tipies ongewenste a', a'', ω neerslae, wat die elastiese modulus verhoog. Nie-giftige Sn is gerapporteer as 'n effektiewe onderdrukker van a', a'' en ω presipitate. Verder is gerapporteer dat toenemende Sn-inhoud die elastiese modulus verlaag. In hierdie studie is die "cluster plus goma atoom" (CPGA) model gebruik om struktureel stabiele β-Ti legerings te ontwikkel deur die byvoeging van Sn. Boogsmelting is uitgevoer om die legerings te vervaardig. Die effek van die vervanging van Mo-atome met 0.4 en 0.5 Sn-atome op die mikrostruktuur en meganiese eienskappe van $[(Mo,Sn)(Ti)_{14}](Nb)_1$-legerings is ondersoek. Die mikrostruktuur van die legerings het groot gelykassige beta-korrels vertoon met die $[(Mo_{0.6}Sn_{0.4})(Ti)_{14}](Nb)_1$ en $[(Mo_{0.5}Sn_{0.5})(Ti)_{14}](Nb)_1$ legerings wat substrukture toon . Die XRD-resultate het getoon dat die legerings uit die β-fase bestaan het; die teenwoordigheid van a'' is egter in die $[(Mo_{0.6}Sn_{0.4})(Ti)_{14}](Nb)_1$-legering waargeneem. Die studie het getoon dat vervanging van 0.5 Mo-atome met 0.5 atome Sn om die $[(Mo_{0.5}Sn_{0.5})(Ti)_{14}](Nb)_1$-kluster te vorm, 'n elastiese modulus van 49 GPa tot gevolg gehad het.

1. INTRODUCTION

Titanium (Ti) and its alloys are commonly used as orthopaedic implants owing to their superior corrosion and fatigue resistance, biocompatibility, mechanical qualities, and lower modulus of elasticity when compared with the conventional metallic biomaterials such as stainless steel and Co-Cr based alloys (Dehghan-Manshadi et al., 2020a; Li & Nam, 2019; Vieira Nunes et al., 2020), [9]. Because of these characteristics, Ti alloys are great candidates for structural components in hard-tissue engineering, such as orthopaedic implants (Dehghan-Manshadi et al., 2020). When it comes to the selection of materials for biomedical uses in orthopaedic implants, among the mechanical properties, Young's modulus is one of the most crucial factors owing to the fact that low values (closer to that of bone ≈10-40 GPa) allow a better distribution of stresses, whereas significantly higher values can result in the stress-shielding effect, which can in turn lead to resorption of the bone and failure of the implant (Dehghan-Manshadi et al., 2020; Jha & Dulikravich, 2021; Moshokoa et al., 2019; Raquel et al., 2017).

Depending on the phase, Ti alloys can be classified into a, $a + \beta$, and β-type alloys. Among these alloys, the $a+\beta$ Ti-6Al-4V alloy is the most commonly used Ti alloy in orthopaedic applications. Even though this alloy has a lower Young's modulus than the conventional orthopaedic implant materials (stainless steel ~ 180 GPa & Co-Cr ~ 210 GPa) (Niinomi & Nakai, 2011), its Young's modulus (~ 110 GPa) is still higher than that of human bone (10-40 GPa) (Jha & Dulikravich, 2021; Niinomi, 2019; Qu et al., 2018). Furthermore, the observed release of V and Al ions from Ti-6Al-4V in the human body limits the biomedical application of the alloy and those similar to it ((Dehghan-Manshadi et al., 2020; Raquel et al., 2017). Studies have shown that the release of small amounts of V and Al in the human body may induce cytotoxic effects and neurological disorders such as Alzheimer's (Moshokoa et al., 2019). This shortcoming has led to the development of new Ti-based alloys consisting of non-toxic β stabilising alloying elements (Mo, Nb, Ta, Cr etc.) and good mechanical properties. These elements are known to segregate easily in titanium alloys; however, much effort has been made to reduce or eliminate the segregation of the alloys (Emura et al., 2020; Hanada et al., 2021; Min et al., 2012; Zhou et al., n.d.). The Young's modulus of $a + \beta$ Ti6Al4V alloy is higher than that of β-type titanium alloys. Therefore, β-type titanium alloys are advantageous for the development of titanium alloys with low Young's modulus for biomedical applications (Dehghan-Manshadi et al., 2020; Nakai et al., 2011).

Various phases such as a' and a'' (martensitic) phase and the ω (omega) phase can form in the metastable β alloys (Bönisch et al., 2017; Hildyard, 2019). The precipitation of these phases increases the Young's modulus because Young's moduli of these phases is much higher than that of the β matrix phase. The ω phase precipitation significantly increases the strength and Young's modulus of the alloy compared with the martensitic phase (Fernandes et al., 2016; Jha & Dulikravich, 2021). It is therefore paramount that this phase be controlled/supressed in β-type titanium biomedical alloys (E. L. Pang et al., 2018). The addition of neutral elements such as Zr and Sn has been said to supress the precipitation of the ω, a' and a'' phases and decrease the Young's modulus (Jha & Dulikravich, 2021; E. L. Pang et al., 2018).

Obtaining a stable β structure with a low elastic modulus from multi-component systems has been found to be a challenge. In order to mitigate the composition complexity that comes with multi-component systems, the cluster-plus-glue-atom (CPGA) model, which provides a material's basic compositional and structural information in its cluster formula [(center atom) -(shell atoms)$_{14}$](glue atoms)$_{1-8}$] has been introduced as a design approach. Elements are placed in the formula based on their interaction, which is characterised by their enthalpy of mixing (ΔH). Elements with a negative ΔH occupy preferentially the cluster center – e.g., Mo (– 4 kJ/mol) and Sn (– 21 kJ/mol) – while elements with a positive ΔH are assigned to the glue site – e.g., Nb (2 kJ/mol) – and elements with an ΔH of zero (0) – e.g., Ti (0 kJ/mol) – are placed in the cluster shell. Through proper placement of the alloying elements in the cluster formula, this model can design alloys with high β stability and low elastic modulus (Jiang et al., 2017; C. Pang et al., 2015; Raganya, 2020; Wang et al., 2013, 2015). In this paper, we use the CPGA model with cluster formula [(Mo$_{1-x}$,Sn$_x$)(Ti)$_{14}$](Nb)$_1$ to investigate the effect of Sn addition on the microstructure and mechanical properties of Ti-Mo-Nb alloys.

2. METHODOLOGY

2.1. Starting materials

The starting materials used in this study were angular shaped Ti powder (-45 μm) with 99.5% purity, angular shaped Nb powder (-5 μm) with a purity of 99.8%, spherical shaped Mo powder (-150 μm) with a purity of 99.9%, and spherical shaped Sn powder (-150 μm) with a purity of 99.9%. The Ti, and Nb powders were supplied by Thermo Scientific, while the Mo and Sn powders were supplied by Alfa Aesar.

2.2. Alloy design and fabrication

Three compositions in the Ti–Mo–Nb–Sn system were formulated using the CPGA model using cluster formula $[(Mo_{1-x},Sn_x)(Ti)_{14}](Nb)_1$ where x=0.4 and 0.5. The alloys were then prepared using 100g powders (per alloy) of varying chemical compositions in accordance with the alloy make-up in Table 1. The starting powders were mixed and then compacted into 45 mm diameter button-shaped green compacts using a uniaxial cold compacting machine at 250 bars. The compacts were then melted in an arc furnace with a non-consumable tungsten electrode and water-cooled copper crucible under argon atmosphere, where Ti getters were used to minimise oxidation. The samples were homogenised by inverting and re-melting them at least three times.

Table 1: Chemical composition of the starting alloys

Cluster formula	Composition (wt.%)
$[(Mo)(Ti)_{14}]\ (Nb)_1$	Ti-11.2Mo-10.8Nb
$[(Mo_{0.6}Sn_{0.4})\ (Ti)_{14}]\ (Nb)_1$	Ti-6.6Mo-10.7Nb-5.5Sn
$[(Mo_{0.5}Sn_{0.5})\ (Ti)_{14}]\ (Nb)_1$	Ti-5.5Mo-10.7Nb-6.8Sn

2.3. Microstructure, chemical composition, and phase analysis

A Leica DMI 5000M optical microscope and a Joel JSM-6510 scanning electron microscope (SEM) equipped with Energy-Dispersive X-ray Spectroscopy (EDS) was used to study the microstructure and chemical composition of the samples. Precision-cut samples from as-cast ingots were mounted, ground, and polished in accordance with the ASTM E3-11 standard guide for the preparation of metallographic specimens. Colloidal silica (3 μm) was used for the final polishing. Etching of the samples was performed using Kroll's reagent, which was composed of 3 ml HNO_3, 2 ml HF, and 100 ml distilled water. Phase identification was analysed using a PANalytical Empyrean diffractometer system operated at 45 kV and 40 mA with Cu Ka as an X-ay source with $\lambda1 = 0.1540598$ nm, $\lambda2 = 1.544426$ nm and a scan range of 20 to 90 degrees 2θ.

2.4. Mechanical testing

Vickers micro-hardness measurements were conducted using a Vickers micro-hardness tester (FM-700, micro-indenter with a square base pyramid tip). A load of 500 g and dwell time of 15 s were used, and five indentations were made on each sample. Tensile testing of the alloys was performed on an Instron 1342 mechanical testing machine in accordance with the ASTM E8/E8M standard test method for tension testing of metallic materials. Figure 1 shows the dimensions of the tensile specimen. Testing was done at a speed of 0.5 mm/sec using three test specimen per alloy.
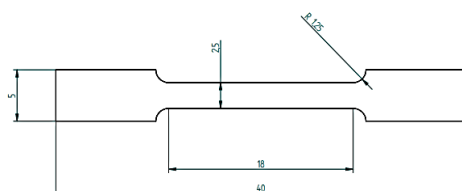

Figure 1: Dimensions of tensile speciment

3. RESULTS

3.1. Microstructure, chemical composition, and phase analysis

Figure 2 depicts optical images of the microstructure of the alloys. It is clear that all of the samples presented large equiaxed β grains. The microstructures of the alloys containing Sn additions (Figures 2(b) and (c)) revealed sub-grain structures within the primary grains upon etching. The alloy with a low Sn content ($[(Mo_{0.6}Sn_{0.4}) (Ti)_{14}] (Nb)_1$) presented the most sub-grain structures. As the Sn content was increased to 0.5 atoms, the structures were seen to diminish. The appearance of such structures in Ti alloys is known to occur during work-hardened alloy recovery (Raganya, 2020), but have also been reported in as-cast metastable β-type Ti alloys, and were attributed to compositional differences (Lin et al., 2017; Ozan et al., 2017).
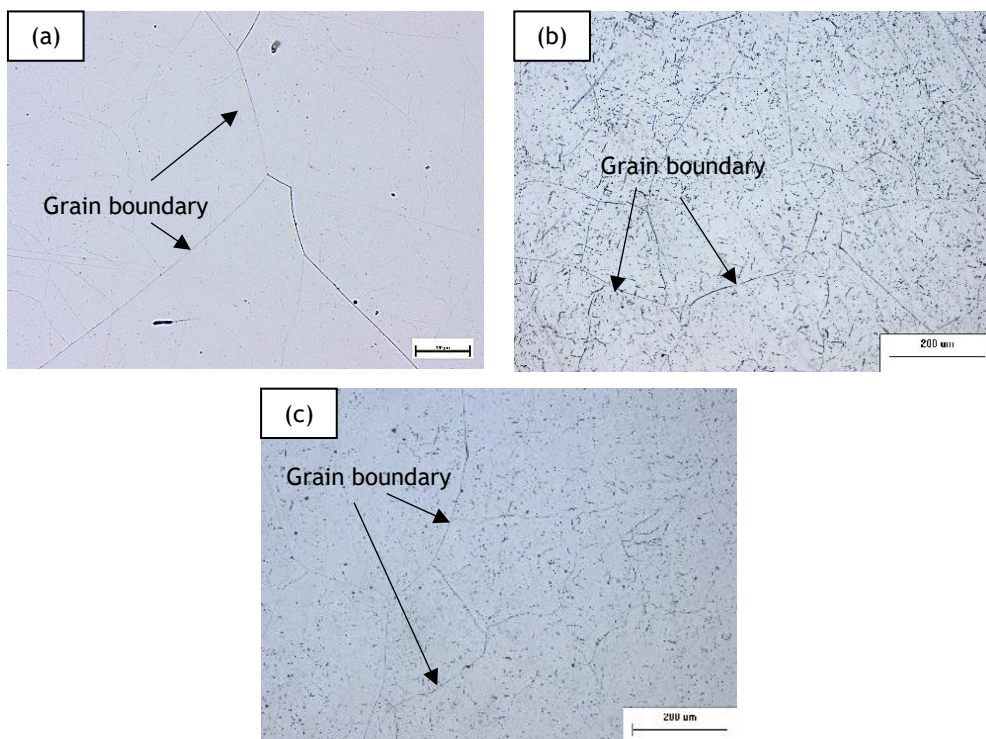

Figure 2: Optical micrographs of the alloys (a) $[(Mo)(Ti)_{14}] (Nb)_1$, (b) $[(Mo_{0.6}Sn_{0.4}) (Ti)_{14}] (Nb)_1$ and (c) $[(Mo_{0.5}Sn_{0.5}) (Ti)_{14}] (Nb)_1$ x100

The chemical compositions of the samples are shown in Table 2. The results suggest that the measured compositions were very close to the nominal compositions.

Table 2: Nominal and measured compositions of the alloys (wt. %)

Nominal composition	Measured composition			
	Ti	Mo	Nb	Sn
Ti-11.2Mo-10.8Nb	Bal.	10.89	10.97	0
Ti-6.6Mo-10.7Nb-5.5Sn	Bal.	6.17	10.32	5.58
Ti-5.5Mo-10.7Nb-6.8Sn	Bal.	5.44	9.97	7.01

Alloying elements such as Mo, Nb, and Sn are known to segregate effortlessly during solidification in Ti alloys (Emura et al., 2020; Liu et al., 2019; Min et al., 2012; Ruzic et al., 2018; Zhou et al., n.d.); consequently, EDS mapping of the as-cast alloys was performed to assess for chemical homogeneity. The EDS mapping in Figure 3 shows that all of the elements were evenly distributed, with no substantial enrichment or depletion in the alloys.
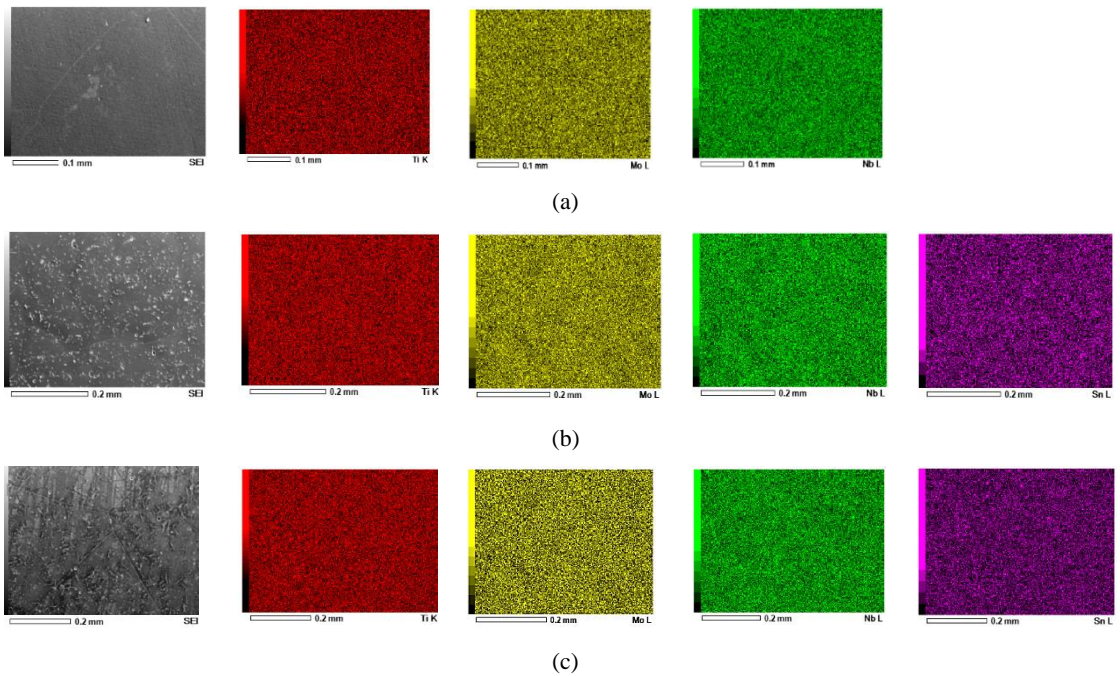

(a)

(b)

(c)

Figure 3: EDS mapping of Ti, Mo, Nb, and Sn distribution in the alloys (a) $[(Mo)(Ti)_{14}]$ $(Nb)_1$, (b) $[(Mo_{0.6}Sn_{0.4})$ $(Ti)_{14}]$ $(Nb)_1$ and (c) $[(Mo_{0.5}Sn_{0.5})$ $(Ti)_{14}]$ $(Nb)_1$

3.2. XRD analysis

Figure 4 shows the X-ray diffraction patterns of the alloys. The $[(Mo)(Ti)_{14}](Nb)_1$ and $[(Mo_{0.5}Sn_{0.5})(Ti)_{14}](Nb)_1$ alloys exhibited β phase diffraction peaks, whereas the $[(Mo_{0.6}Sn_{0.4})(Ti)_{14}](Nb)_1$ alloy exhibited $β$ phase diffraction peaks and peaks corresponding to the secondary martensitic $α''$ phase. Given that the solidification in the copper mould resulted in rapid solidification and cooling, it was to be expected that the final microstructure could consist of metastable phases, depending on the content of the $β$ stabilising elements, as indicated by (Moraes et al., 2014). The results indicate that the substitution of 0.4 Mo atoms with Sn resulted in destabilisation of the $β$ phase. When Mo and Sn shared equal atoms in the cluster site of the model $([(Mo_{0.5}Sn_{0.5})(Ti)_{14}](Nb)_1)$, the $α''$ peaks disappeared, demonstrating that increasing the number of Sn atoms resulted in the structural stability of the $β$ phase. The stabilisation of the $β$-phase in Ti alloys through additions of Sn has been reported in the works of Wang et al. (Wang et al., 2015) on Ti-Mo-Nb-Zr Sn, Endoh et al. (Endoh et al., 2017) on Ti-Mo-Sn, Ijaz et al. (Ijaz et al., 2014) on Ti-Mo-Nb-Sn, and Guo et al. (Guo et al., 2015) on Ti-Nb-Sn alloys.
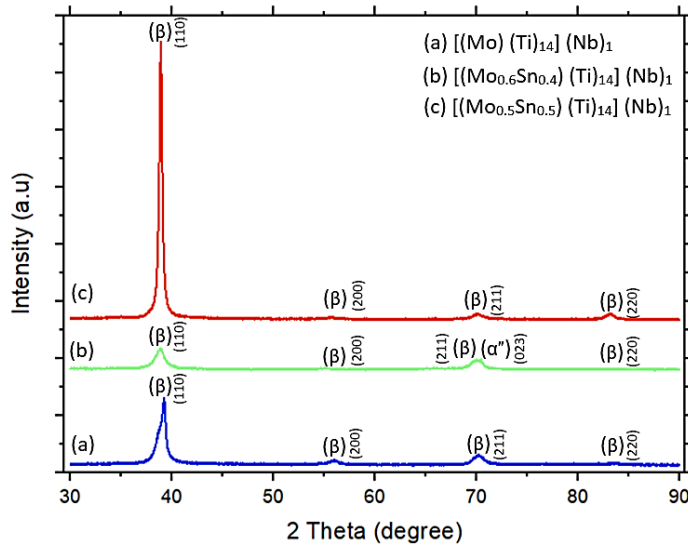
Figure 4: XRD patters of the alloys (a) [(Mo)(Ti)$_{14}$] (Nb)$_1$, (b) [(Mo$_{0.6}$Sn$_{0.4}$) (Ti)$_{14}$] (Nb)$_1$, and (c) [(Mo$_{0.5}$Sn$_{0.5}$) (Ti)$_{14}$] (Nb)$_1$

3.3. Mechanical testing

Figure 5 shows the measured Vickers hardness and elastic modulus of the alloys. The results show that the addition of 0.4 Sn atoms in the cluster formula [(Mo$_{1-x}$,Sn$_x$)(Ti)$_{14}$](Nb)$_1$ resulted in an increase in both the micro-hardness and elastic modulus values. The hardness increased from 384 to 391 HV, whereas the elastic modulus increased from 57 to 67 GPa. The elastic modulus was strongly affected by secondary phase precipitation. Small amounts of α'' and ω phases have been reported to increase the elastic modulus of metastable β-type Ti alloys significantly (Fernandes et al., 2016; Jha & Dulikravich, 2021). As a result, the α'' secondary phase observed in the XRD pattern in the [(Mo$_{0.6}$Sn$_{0.4}$)(Ti)$_{14}$](Nb)$_1$ alloy contributed to an increase in the micro-hardness and elastic modulus. It is well-known that the mechanical properties of titanium alloys are related to the morphology and fractions of phases in the microstructure. With increased Sn addition to form the [(Mo$_{0.5}$Sn$_{0.5}$)(Ti)$_{14}$](Nb)$_1$ alloy, the proportion of α'' phase diminished, as shown by the XRD patterns. The hardness and elastic modulus in this alloy were seen to decrease from 391 to 372 HV and from 67 to 49 GPa respectively. Since the hardness and elastic modulus of the α'' phase was higher than that of the β phase, the decrease in hardness and elastic modulus in the[(Mo$_{0.5}$Sn$_{0.5}$)(Ti)$_{14}$](Nb)$_1$ alloy may be attributed to the inhibition of Sn addition on the formation of the α'' and possibly the ω phase. However, the ω phase is difficult to detect on XRD without the use of slow scanning speeds. The decrease in hardness and elastic modulus through the addition of Sn has been reported by Xie et al. (Xie et al., 2022) on Ti-Nb-Sn, Hao et al. (Hao et al., 2006) on Ti-Nb-Zr-Sn, Zhang et al. (Zhang et al., 2012) on Ti-Nb=Mo-Sn, and (Moraes et al., 2014) on Ti-Nb-Sn alloys.
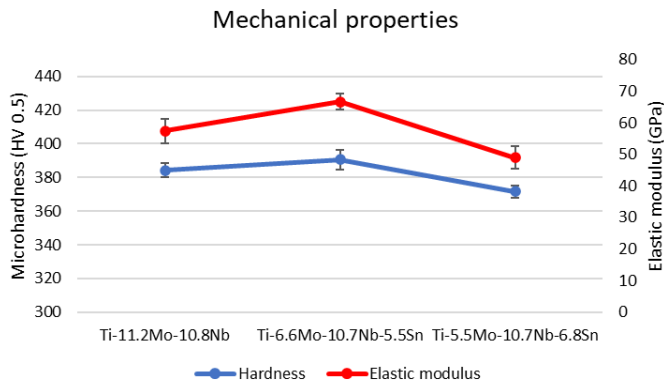

Figure 5: Hardness and elastic modulus of the alloys

4. CONCLUSIONS

In this study, we used the cluster-plus-glue-atom (CPGA) model with cluster formula $[(Mo_{1-x},Sn_x)(Ti)_{14}](Nb)_1$ to investigate the effect of Sn on the microstructure, and mechanical properties of Ti-Mo-Nb alloys. Based on the findings, the following can be concluded:

- The microstructures of the formulated alloys consisted of equiaxed β grains with no evidence of any secondary phases.

- XRD analysis showed that substituting 0.4 atoms of Mo with Sn atoms in the cluster shell resulted in the formation of secondary α″ phases. However, further increasing the Sn atom to 0.5 atoms resulted in a highly stable β phase.

- Increasing the content of Sn atoms in the cluster shell resulted in a decrease in the elastic modulus and micro-hardness of the alloy. The $[(Mo_{0.5}Sn_{0.5})(Ti)_{14}](Nb)_1$ obtained the lowest hardness and elastic modulus values of 372 HV and 49 GPa.

REFERENCES

[1] **S. Li & T.-H. Nam**, "Superelasticity and tensile strength of Ti-Zr-Nb-Sn alloys with high Zr content for biomedical applications," *Intermetallics (Barking)*, vol. 112, June, 2019. doi: 10.1016/j.intermet.2019.106545.

[2] **A. R. Vieira Nunes, S. Borborema, L. S. Araújo, L. Malet, J. Dille, & L. Henrique de Almeida**, "Influence of thermo-mechanical processing on structure and mechanical properties of a new metastable β Ti–29Nb–2Mo–6Zr alloy with low Young's modulus," *Journal of Alloys and Compounds*, vol. 820, 153078, 2020. doi: 10.1016/j.jallcom.2019.153078.

[3] **A. Dehghan-Manshadi, D. Kent, D. StJohn, & M. Dargusch**, "Properties of powder metallurgy-fabricated oxygen-containing Beta Ti–Nb–Mo–Sn–Fe alloys for biomedical applications," *Advanced Engineering Materials*, vol. 22, no. 3, pp. 1–6, 2020. doi: 10.1002/adem.201901229.

[4] **A. Raquel, V. Nunes, S. Borborema, C. Angelo, & L. Sales**, "Microstructure and mechanical properties of Ti-12Mo-8Nb alloy hot swaged and treated for orthopedic applications," *Materials Research,* vol. 20, pp. 526–531, 2017.

[5] **N. Moshokoa, L. Raganya, B. Obadele, P. Olubambi, & R. Machaka**, "Effects of Mo content on the microstructural and mechanical properties of as-cast Ti-Mo alloys," in *IOP Conference Series: Materials Science and Engineering*, Nov. 2019, vol. 655, no. 1. doi: 10.1088/1757-899X/655/1/012015.

[6] **R. Jha & G. S. Dulikravich**, "Discovery of new Ti-based alloys aimed at avoiding/minimizing formation of α″ and ω-phase using CALPHAD and artificial intelligence," *Metals (Basel)*, vol. 11, no. 1, pp. 1–15, 2021. doi: 10.3390/met11010015.

[7] **M. Niinomi & M. Nakai**, "Titanium-based biomaterials for preventing stress shielding between implant devices and bone," *International Journal of Biomaterials*, vol. 2011, 83658, 2011. doi: 10.1155/2011/836587.

[8] **M. Niinomi**, "Design and development of metallic biomaterials with biological and mechanical biocompatibility," *Journal of Biomedical Materials Research – Part A*, vol. 107, no. 5, pp. 944–954, 2019. doi: 10.1002/jbm.a.36667.

[9] **Y. Qu *et al*.**, "Ti-24Nb-4Zr-8Sn alloy pedicle screw improves internal vertebral fixation by reducing stress-shielding effects in a porcine model," *BioMed Research International*, vol. 2018, no. 1, pp. 1–13, 2018. doi: 10.1155/2018/8639648.

[10] **T. Zhou, G. Itoh, Y. Motohashi, & M. Niinomi**, "Microstructural modification in a beta titanium alloy for implant applications," *Materials Transactions,* Vol. 47, No. 1, pp. 90 to 95, 2006.

[11] **X. H. Min, K. Tsuzaki, S. Emura, & K. Tsuchiya**, "Heterogeneous twin formation and its effect on tensile properties in Ti-Mo based β titanium alloys," *Materials Science and Engineering A*, vol. 554, pp. 53–60, 2012. doi: 10.1016/j.msea.2012.06.009.

[12] **S. Hanada, N. Masahashi, S. Semboshi, & T. K. Jung**, "Low Young's modulus of cold groove-rolled β Ti–Nb–Sn alloys for orthopedic applications," *Materials Science and Engineering A*, vol. 802, 2021. doi: 10.1016/j.msea.2020.140645.

[13] **S. Emura, X. Ji, X. Min, & K. Tsuchiya**, "Effects of Mo segregation on Charpy absorbed energy in Ti-12Mo alloys," *MATEC Web of Conferences*, vol. 321, 11050, 2020. doi: 10.1051/matecconf/202032111050.

[14] **M. Nakai, M. Niinomi, X. Zhao, & X. Zhao**, "Self-adjustment of Young's modulus in biomedical titanium alloys during orthopaedic operation," *Materials Letters*, vol. 65, no. 4, pp. 688–690, 2011. doi: 10.1016/j.matlet.2010.11.006.

[15]   **M. Bönisch** *et al*., "Giant thermal expansion and α-precipitation pathways in Ti-alloys," *Nature Communications*, vol. 8, no. 1, pp. 1–9, 2017. doi: 10.1038/s41467-017-01578-1.

[16]   **E. Hildyard**, "An investigation into the influence of microstructural condition on the superelastic behaviour in Ti-Nb-based alloys," PhD thesis, University of Cambridge, 2019.

[17]   **P. Fernandes** *et al*., "Fabrication of low-cost beta-type Ti – Mn alloys for biomedical applications by metal injection molding process and their mechanical properties," vol. 59, pp. 497–507, 2016. doi: 10.1016/j.jmbbm.2016.02.035.

[18]   **E. L. Pang, E. J. Pickering, S. I. Baik, D. N. Seidman, & N. G. Jones**, "The effect of zirconium on the omega phase in Ti-24Nb-[0–8]Zr (at.%) alloys," *Acta Materialia*, vol. 153, pp. 62–70, 2018. doi: 10.1016/j.actamat.2018.04.016.

[19]   **B. Jiang** *et al*., "Effects of Nb and Zr on structural stabilities of Ti-Mo-Sn-based alloys with low modulus," *Materials Science and Engineering A*, vol. 687, pp. 1–7, 2017. doi: 10.1016/j.msea.2017.01.047.

[20]   **Q. Wang** *et al*., "Microstructures and stability origins of ß-(Ti,Zr)-(Mo,Sn)-Nb alloys with low Young's modulus," *Metallurgical and Materials Transactions A*, vol. 46, no. 9, pp. 3924-3931, 2015. doi: 10.1007/s11661-015-3011-4.

[21]   **Q. Wang, C. Ji, Y. Wang, J. Qiang, & C. Dong**, "ß-Ti alloys with low Young's moduli interpreted by cluster-plus-glue-atom model," *Metallurgical and Materials Transactions A: Physical Metallurgy and Materials Science*, vol. 44, no. 4, pp. 1872–1879, 2013. doi: 10.1007/s11661-012-1523-8.

[22]   **M. L. Raganya**, "Design of Ti-Mo-Nb-Zr alloys with low elastic modulus using cluster-plus-glue atom model," PhD thesis, University of Johannesburg, 2020. https://hdl.handle.net/10210/479516.

[23]   **C. Pang, B. Jiang, Y. Shi, Q. Wang, & C. Dong**, "Cluster-plus-glue-atom model and universal composition formulas [cluster](glue atom)x for BCC solid solution alloys," *Journal of Alloys and Compounds*, vol. 652, pp. 63–69, 2015. doi: 10.1016/j.jallcom.2015.08.209.

[24]   **S. Ozan, J. Lin, Y. Li, & C. Wen**, "New Ti-Ta-Zr-Nb alloys with ultrahigh strength for potential orthopedic implant applications," *Journal of the Mechanical Behavior of Biomedical Materials*, vol. 75, pp. 119–127, 2017. doi: 10.1016/j.jmbbm.2017.07.011.

[25]   **J. Lin** *et al*., "Effects of solution treatment and aging on the microstructure, mechanical properties, and corrosion resistance of a ß type Ti–Ta–Hf–Zr alloy," *RSC Advances*, vol. 7, no. 20, pp. 12309–12317, 2017. doi: 10.1039/C6RA28464G.

[26]   **J. Ruzic, S. Emura, X. Ji, & I. Watanabe**, "Mo segregation and distribution in Ti–Mo alloy investigated using nanoindentation," *Materials Science and Engineering A*, vol. 718, pp. 48–55, 2018. doi: 10.1016/j.msea.2018.01.098.

[27]   **X. Liu, G. Feng, Y. Zhou, & Q. Fan**, "Macrosegregation and the underlying mechanism in Ti-6.5Al-1.0Cr-0.5Fe-6.0Mo-3.0Sn-4.0Zr alloy," *Progress in Natural Science: Materials International*, vol. 29, no. 2, pp. 224–230, 2019. doi: 10.1016/j.pnsc.2019.02.006.

[28]   **P. E. L. Moraes, R. J. Contieri, E. S. N. Lopes, A. Robin, & R. Caram**, "Effects of Sn addition on the microstructure, mechanical properties and corrosion behavior of Ti-Nb-Sn alloys," *Materials Characterization*, vol. 96, pp. 273-281, 2014. doi: 10.1016/j.matchar.2014.08.014.

[29]   **K. Endoh, M. Tahara, T. Inamura, & H. Hosoda**, "Effect of Sn and Zr addition on the martensitic transformation behavior of Ti-Mo shape memory alloys," *Journal of Alloys and Compounds*, vol. 695, pp. 76–82, 2017. doi: 10.1016/j.jallcom.2016.10.108.

[30]   **M. F. Ijaz, H. Y. Kim, H. Hosoda, & S. Miyazaki**, "Effect of Sn addition on stress hysteresis and superelastic properties of a Ti-15Nb-3Mo alloy," *Scripta Materialia*, vol. 72-73, pp. 29-32, 2014. doi: 10.1016/j.scriptamat.2013.10.007.

[31]   **S. Guo, Q. Meng, X. Zhao, Q. Wei, & H. Xu**, "Design and fabrication of a metastable ß-type titanium alloy with ultralow elastic modulus and high strength," *Scientific Reports*, vol. 5, no. 1, 14688, 2015. doi: 10.1038/srep14688.

[32]   **F. Xie, H. Yang, J. Huang, J. Yu, & X. He**, "Sn content effects on microstructure, mechanical properties and tribological behavior of biomedical Ti-Nb-Sn alloys fabricated by powder metallurgy," *Metals (Basel)*, vol. 12, no. 2, 2022. doi: 10.3390/met12020255.

[33]   **Y. L. Hao, S. J. Li, S. Y. Sun, & R. Yang**, "Effect of Zr and Sn on Young's modulus and superelasticity of Ti-Nb-based alloys," *Materials Science and Engineering A*, vol. 441, no. 1–2, pp. 112-118, 2006. doi: 10.1016/j.msea.2006.09.051.

[34]   **D. C. Zhang, S. Yang, M. Wei, Y. F. Mao, C. G. Tan, & J. G. Lin**, "Effect of Sn addition on the microstructure and superelasticity in Ti-Nb-Mo–Sn alloys," *Journal of the Mechanical Behavior of Biomedical Materials*, vol. 13, pp. 156–165, 2012. doi: 10.1016/j.jmbbm.2012.04.017.